E-ISSN: 2708-3977
P-ISSN: 2708-3969
IJEDC 2021; 2(2): 43-50

www.datacomjournal.com
Received: 19-06-2021
Accepted: 26-07-2021

EL Pankratov
[1.] Nizhny Novgorod State University, 23 Gagarin Avenue, Nizhny Novgorod, 603950, Russia
[2.] Nizhny Novgorod State Technical University, 24 Minin Street, Nizhny Novgorod, 603950, Russia

Correspondence
EL Pankratov
[1.] Nizhny Novgorod State University, 23 Gagarin Avenue, Nizhny Novgorod, 603950, Russia
[2.] Nizhny Novgorod State Technical University, 24 Minin Street, Nizhny Novgorod, 603950, Russia

On prognosis of manufacturing of a four stages distributed amplifier: Accounting of mismatch-induced stress and porosity of materials on technological process

EL Pankratov

Abstract
In this paper we introduce an approach to increase density of field-effect transistors framework a four stages distributed amplifier. Framework the approach we consider manufacturing the amplifier in heterostructure with specific configuration. Several required areas of the heterostructure should be doped by diffusion or ion implantation. After that dopant and radiation defects should by annealed framework optimized scheme. We also consider an approach to decrease value of mismatch-induced stress in the considered heterostructure. We introduce an analytical approach to analyze mass and heat transport in heterostructures during manufacturing of integrated circuits with account mismatch-induced stress.

Keywords: analytical approach for modelling, four stages distributed amplifier, optimization of manufacturing, accounting of mismatch induced stress and porosity of materials.

Introduction
Rwanda is depending on imports where 100% of fuel used in Rwanda is imported and transport cost is high due to fuel imported. Today Rwanda is promoting E-Mobility where electrical motorcycles, vehicles and bikes are in manufacturing in Rwanda to reduce the emissions and quantity of fuel consumptions (Sweco, 2019) [2].
The E-mobility avoids the use of fuel and promotes the decrease of carbon emissions in environment. Average price of fuel in Rwanda is 1.09 $ and the average vehicles in Kigali city was about 30,000 in 2018. Three companies Ampersand, Safi and Rwanda Electric mobility are targeting to contribute in implementation of this new system of E-Mobility.
Development of urban transport is increasing due to high increase of population in the Cities. Rwanda is targeting 35% of Rwandans to be in cities by 2030. Use of E-vehicles does not need any toxic materials to be manipulated (Gardiner, 2017). E-Mobility optimizes the consumption of fuel (Johnson, 2017). The city can be cooled down by 2oC due to a use of E-Mobility (Zielinski, 2015). The E-System contributes on city cleanness and quit (Gardiner, 2017), innovation in technology should be applied for the system to perform in relation with battery life span and cost (Köhler *et al*., 2009) [3]. The Charging infrastructures and their performance for battery electric vehicles should be provided around the city to meet the economy of scale (van Bree *et al*., 2010). The electric vehicles contribute on reduction of CO2-emissions only when the source of energy does not depend on combustion coals (Zimmer *et al*., 2011) [4]. The city of Kigali to be carbon neutral, the e-vehicles, moto, scooters and bikes have been manufactured and started to operate in the city (Ruud, 2019), Electric cars require few parts compared to combustion engine cars (Barthel *et al*. 2010). The study conducted in 2006 indicated that more that 20% of Co2 emissions produced in urban zones was from urban mobility (Schoemaker *et al*., 2006); the mileage consumed by combustion engine vehicles will be substituted by electrical and the government of Rwanda has targeted electric access at 100% by 2024 (Usaid, 2020).

2. Materials and Methodology
The materials in this paper are electrical vehicles, E-bikes and E-motors in Kigali city. The methodology used to collect data is on site observation and survey applied in different points of the city. The sample size was calculated based on city population with confidence level

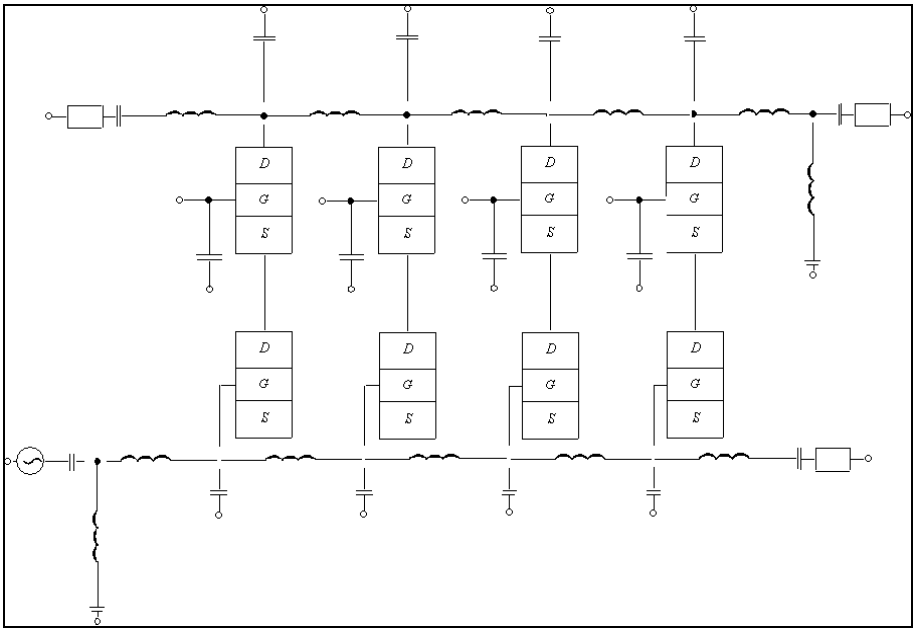

Fig 1*a*: Structure of the considered amplifier [19].

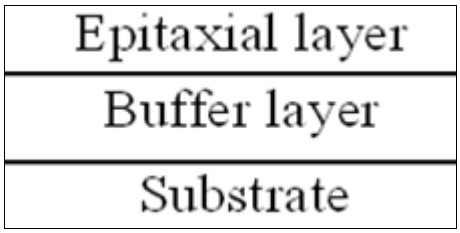

Fig 1b: Heterostructure with a substrate, epitaxial layers and buffer layer (view from side)

Method of solution

To solve our aim we determine and analyzed spatio-temporal distribution of concentration of dopant in the considered heterostructure. We determine the distribution by solving the second Fick's law in the following form [1, 20-23].

$$\frac{\partial C(x,y,z,t)}{\partial t} = \frac{\partial}{\partial x}\left[D\frac{\partial C(x,y,z,t)}{\partial x}\right] + \frac{\partial}{\partial y}\left[D\frac{\partial C(x,y,z,t)}{\partial y}\right] + \frac{\partial}{\partial z}\left[D\frac{\partial C(x,y,z,t)}{\partial z}\right] +$$

$$+\Omega\frac{\partial}{\partial x}\left[\frac{D_S}{kT}\nabla_S\mu_1(x,y,z,t)\int_0^{L_z}C(x,y,W,t)dW\right] +$$

$$+\Omega\frac{\partial}{\partial y}\left[\frac{D_S}{kT}\nabla_S\mu_1(x,y,z,t)\int_0^{L_z}C(x,y,W,t)dW\right] + \quad (1)$$

$$+\frac{\partial}{\partial \vec{r}x}\left[\frac{D_{CS}}{\bar{V}kT}\frac{\partial\mu_2(x,y,z,t)}{\partial x}\right] + \frac{\partial}{\partial \vec{r}y}\left[\frac{D_{CS}}{\bar{V}kT}\frac{\partial\mu_2(x,y,z,t)}{\partial y}\right] + \frac{\partial}{\partial \vec{r}z}\left[\frac{D_{CS}}{\bar{V}kT}\frac{\partial\mu_2(x,y,z,t)}{\partial z}\right]$$

With boundary and initial conditions

$$\left.\frac{\partial C(x,y,z,t)}{\partial x}\right|_{x=0} = 0, \left.\frac{\partial C(x,y,z,t)}{\partial x}\right|_{x=L_x} = 0, \left.\frac{\partial C(x,y,z,t)}{\partial y}\right|_{y=0} = 0, C$$

$(x,y,z,0)=f_C\ (x,y,z)$,

$$\left.\frac{\partial C(x,y,z,t)}{\partial y}\right|_{x=L_y} = 0, \left.\frac{\partial C(x,y,z,t)}{\partial z}\right|_{z=0} = 0, \left.\frac{\partial C(x,y,z,t)}{\partial z}\right|_{x=L_z} = 0.$$

Here $C(x, y, z, t)$ is the spatio-temporal distribution of concentration of dopant; Ω is the atomic volume of dopant; ∇_s is the symbol of surficial gradient; $\int_0^{L_z} C(x,y,z,t)dz$ is the surficial concentration of dopant on interface between layers of heterostructure (in this situation we assume, that Z-axis is perpendicular to interface between layers of heterostructure); $\mu_1(x, y, z, t)$ and $\mu_2(x, y, z, t)$ are the chemical potential due to the presence of mismatch-induced stress and porosity of material; D and D_S are the coefficients of volumetric and surficial diffusions. Values of dopant diffusions coefficients depends on properties of materials of heterostructure, speed of heating and cooling of materials during annealing and spatio-temporal distribution of concentration of dopant. Dependences of dopant diffusions coefficients on parameters could be approximated by the following relations [24-26].

$$D_C = D_L(x,y,z,T)\left[1+\xi\frac{C^\gamma(x,y,z,t)}{P^\gamma(x,y,z,T)}\right]\left[1+\varsigma_1\frac{V(x,y,z,t)}{V^*}+\varsigma_2\frac{V^2(x,y,z,t)}{(V^*)^2}\right]$$

$$D_S = D_{SL}(x,y,z,T)\left[1+\xi_S\frac{C^\gamma(x,y,z,t)}{P^\gamma(x,y,z,T)}\right]\left[1+\varsigma_1\frac{V(x,y,z,t)}{V^*}+\varsigma_2\frac{V^2(x,y,z,t)}{(V^*)^2}\right] \quad (2)$$

Here $D_L\ (x, y, z, T)$ and $D_{LS}\ (x, y, z, T)$ are the spatial (due to accounting all layers of heterostruicture) and temperature (due to Arrhenius law) dependences of dopant diffusion coefficients; T is the temperature of annealing; $P\ (x, y, z, T)$ is the limit of solubility of dopant; parameter γ depends on properties of materials and could be integer in the following interval $\gamma \in$ [1,3, 24]; $V\ (x, y, z, t)$ is the spatio-temporal distribution of concentration of radiation vacancies; V^* is the

equilibrium distribution of vacancies. Concentration dependence of dopant diffusion coefficient has been described in details in [24]. Spatio-temporal distributions of concentration of point radiation defects have been determined by solving the following system of equations [20-23, 25, 26].

$$\frac{\partial \rho(x,y,z,t)}{\partial t} = \frac{\partial}{\partial x}\left[D_\rho(x,y,z,T)\frac{\partial \rho(x,y,z,t)}{\partial x}\right] + \frac{\partial}{\partial y}\left[D_\rho(x,y,z,T)\frac{\partial \rho(x,y,z,t)}{\partial y}\right] +$$

$$+\frac{\partial}{\partial z}\left[D_\rho(x,y,z,T)\frac{\partial \rho(x,y,z,t)}{\partial z}\right] - k_{\rho,\rho}(x,y,z,T)\rho^2(x,y,z,t) - k_{I,V}(x,y,z,T)\times$$

$$\times I(x,y,z,t)V(x,y,z,t) + \Omega\frac{\partial}{\partial x}\left[\frac{D_{\rho S}}{kT}\nabla_S\mu(x,y,z,t)\int_0^{L_z}\rho(x,y,W,t)dW\right] +$$

$$+\Omega\frac{\partial}{\partial y}\left[\frac{D_{\rho S}}{kT}\nabla_S\mu(x,y,z,t)\int_0^{L_z}\rho(x,y,W,t)dW\right] + \frac{\partial}{\partial x}\left[\frac{D_{\rho S}}{\bar{V}kT}\frac{\partial \mu_2(x,y,z,t)}{\partial x}\right] +$$

$$+\frac{\partial}{\partial y}\left[\frac{D_{\rho S}}{\bar{V}kT}\frac{\partial \mu_2(x,y,z,t)}{\partial y}\right] + \frac{\partial}{\partial z}\left[\frac{D_{\rho S}}{\bar{V}kT}\frac{\partial \mu_2(x,y,z,t)}{\partial z}\right] \quad (3)$$

With boundary and initial conditions

$$\left.\frac{\partial \rho(x,y,z,t)}{\partial x}\right|_{x=0} = 0, \left.\frac{\partial \rho(x,y,z,t)}{\partial x}\right|_{x=L_x} = 0, \left.\frac{\partial \rho(x,y,z,t)}{\partial y}\right|_{y=0} = 0,$$

$$\left.\frac{\partial \rho(x,y,z,t)}{\partial y}\right|_{y=L_y} = 0, \left.\frac{\partial \rho(x,y,z,t)}{\partial z}\right|_{z=0} = 0, \left.\frac{\partial \rho(x,y,z,t)}{\partial z}\right|_{z=L_z} = 0 \quad (4)$$

$\rho(x, y, z, 0) = f_V(x, y, z)$,

$$V(x_1 + V_n t, y_1 + V_n t, z_1 + V_n t, t) = V_\infty\left(1 + 2\ell\omega/kT\sqrt{x_1^2 + y_1^2 + z_1^2}\right)$$

.

Here $\rho = I,V$; $I(x, y, z, t)$ is the spatio-temporal distribution of concentration of radiation interstitials; I^* is the equilibrium distribution of interstitials; $D_I(x, y, z, T)$, $D_V(x, y, z, T)$, $D_{IS}(x, y, z, T)$, $D_{VS}(x, y, z, T)$ are the coefficients of volumetric and surficial diffusions of interstitials and vacancies, respectively; terms $V^2(x, y, z, t)$ and $I^2(x, y, z, t)$ correspond to generation of divacancies and diinterstitials, respectively (see, for example, [26] and appropriate references in this book); $k_{I,V}(x, y, z, T)$, $k_{I,I}(x, y, z, T)$ and $k_{V,V}(x, y, z, T)$ are the parameters of recombination of point radiation defects and generation of their complexes; k is the Boltzmann constant; $\omega = a^3$, a is the interatomic distance; ℓ is the specific surface energy. To account porosity of buffer layers we assume, that porous are approximately cylindrical with average values $r = \sqrt{x_1^2 + y_1^2}$ and z_1 before annealing [23]. With time small pores decomposing on vacancies. The vacancies absorbing by larger pores [27]. With time large pores became larger due to absorbing the vacancies and became more spherical [27]. Distribution of concentration of vacancies in heterostructure, existing due to porosity, could be determined by summing on all pores, i.e.

$$V(x,y,z,t) = \sum_{i=0}^{l}\sum_{j=0}^{m}\sum_{k=0}^{n}V_p(x + i\alpha, y + j\beta, z + k\chi, t),$$

$$R = \sqrt{x^2 + y^2 + z^2}.$$

Here α, β and χ are the average distances between centers of pores in directions x, y and z; l, m and n are the quantity of pores inappropriate directions.

Spatio-temporal distributions of divacancies $\Phi_V(x, y, z, t)$ and diinterstitials $\Phi_I(x, y, z, t)$ could be determined by solving the following system of equations [25, 26].

$$\frac{\partial \Phi_\rho(x,y,z,t)}{\partial t} = \frac{\partial}{\partial x}\left[D_{\Phi_\rho}(x,y,z,T)\frac{\partial \Phi_\rho(x,y,z,t)}{\partial x}\right] + \frac{\partial}{\partial y}\left[D_{\Phi_\rho}(x,y,z,T)\frac{\partial \Phi_\rho(x,y,z,t)}{\partial y}\right] +$$

$$+\frac{\partial}{\partial z}\left[D_{\Phi_\rho}(x,y,z,T)\frac{\partial \Phi_\rho(x,y,z,t)}{\partial z}\right] + \Omega\frac{\partial}{\partial x}\left[\frac{D_{\Phi_\rho S}}{kT}\nabla_S\mu_1(x,y,z,t)\int_0^{L_z}\Phi_\rho(x,y,W,t)dW\right] +$$

$$+\Omega\frac{\partial}{\partial y}\left[\frac{D_{\Phi_\rho S}}{kT}\nabla_S\mu_1(x,y,z,t)\int_0^{L_z}\Phi_\rho(x,y,W,t)dW\right] + k_{\rho,\rho}(x,y,z,T)\rho^2(x,y,z,t) +$$

$$+\frac{\partial}{\partial x}\left[\frac{D_{\Phi_\rho S}}{\bar{V}kT}\frac{\partial \mu_2(x,y,z,t)}{\partial x}\right] + \frac{\partial}{\partial y}\left[\frac{D_{\Phi_\rho S}}{\bar{V}kT}\frac{\partial \mu_2(x,y,z,t)}{\partial y}\right] + \frac{\partial}{\partial z}\left[\frac{D_{\Phi_\rho S}}{\bar{V}kT}\frac{\partial \mu_2(x,y,z,t)}{\partial z}\right] +$$

$$+k_\rho(x,y,z,T)\rho(x,y,z,t) \quad (5)$$

With boundary and initial conditions

$$\left.\frac{\partial \Phi_\rho(x,y,z,t)}{\partial x}\right|_{x=0} = 0, \left.\frac{\partial \Phi_\rho(x,y,z,t)}{\partial x}\right|_{x=L_x} = 0, \left.\frac{\partial \Phi_\rho(x,y,z,t)}{\partial y}\right|_{y=0} = 0,$$

$$\left.\frac{\partial \Phi_\rho(x,y,z,t)}{\partial y}\right|_{y=L_y} = 0, \left.\frac{\partial \Phi_\rho(x,y,z,t)}{\partial z}\right|_{z=0} = 0, \left.\frac{\partial \Phi_\rho(x,y,z,t)}{\partial z}\right|_{z=L_z} = 0, \quad (6)$$

$\Phi_\rho(x,y,z,0) = f_{\Phi\rho}(x, y, z)$.

Here $D_{\Phi I}(x, y, z, T)$, $D_{\Phi V}(x, y, z, T)$, $D_{\Phi IS}(x, y, z, T)$ and $D_{\Phi VS}(x, y, z, T)$ are the coefficients of volumetric and surficial diffusions of complexes of radiation defects; $k_I(x, y, z, T)$ and $k_V(x, y, z, T)$ are the parameters of decay of

complexes of radiation defects. Chemical potential μ_1 in Eq.(1) could be determine by the following relation [20].

$$\mu_1=E(z)\Omega\sigma_{ij}\,[u_{ij}(x, y, z, t)+u_{ji}(x, y, z, t)]/2, \quad (7)$$

Where $E(z)$ is the Young modulus, σ_{ij} is the stress tensor; $u_{ij}=\frac{1}{2}\left(\frac{\partial u_i}{\partial x_j}+\frac{\partial u_j}{\partial x_i}\right)$ is the deformation tensor; u_i, u_j are the components $u_x(x, y, z, t)$, $u_y(x, y, z, t)$ and $u_z(x, y, z, t)$ of the displacement vector $\vec{u}(x,y,z,t)$; x_i, x_j are the coordinate x, y, z. The Eq. (3) could be transform to the following form

$$\mu(x,y,z,t)=\left[\frac{\partial u_i(x,y,z,t)}{\partial x_j}+\frac{\partial u_j(x,y,z,t)}{\partial x_i}\right]\left\{\frac{1}{2}\left[\frac{\partial u_i(x,y,z,t)}{\partial x_j}+\frac{\partial u_j(x,y,z,t)}{\partial x_i}\right]-\right.$$

$$\left.-\varepsilon_0\delta_{ij}+\frac{\sigma(z)\delta_{ij}}{1-2\sigma(z)}\left[\frac{\partial u_k(x,y,z,t)}{\partial x_k}-3\varepsilon_0\right]-K(z)\beta(z)[T(x,y,z,t)-T_0]\delta_{ij}\right\}\frac{\Omega}{2}E(z),$$

Where σ is Poisson coefficient; $\varepsilon_0 = (a_s\text{-}a_{EL})/a_{EL}$ is the mismatch parameter; a_s, a_{EL} are lattice distances of the substrate and the epitaxial layer; K is the modulus of uniform compression; β is the coefficient of thermal expansion; T_r is the equilibrium temperature, which coincide (for our case) with room temperature. Components of displacement vector could be obtained by solution of the following equations [21].

$$\begin{cases}\rho(z)\frac{\partial^2 u_x(x,y,z,t)}{\partial t^2}=\frac{\partial\sigma_{xx}(x,y,z,t)}{\partial x}+\frac{\partial\sigma_{xy}(x,y,z,t)}{\partial y}+\frac{\partial\sigma_{xz}(x,y,z,t)}{\partial z}\\ \rho(z)\frac{\partial^2 u_y(x,y,z,t)}{\partial t^2}=\frac{\partial\sigma_{yx}(x,y,z,t)}{\partial x}+\frac{\partial\sigma_{yy}(x,y,z,t)}{\partial y}+\frac{\partial\sigma_{yz}(x,y,z,t)}{\partial z}\\ \rho(z)\frac{\partial^2 u_z(x,y,z,t)}{\partial t^2}=\frac{\partial\sigma_{zx}(x,y,z,t)}{\partial x}+\frac{\partial\sigma_{zy}(x,y,z,t)}{\partial y}+\frac{\partial\sigma_{zz}(x,y,z,t)}{\partial z}\end{cases} \quad (8)$$

Where

$$\sigma_{ij}=\frac{E(z)}{2[1+\sigma(z)]}\left[\frac{\partial u_i(x,y,z,t)}{\partial x_j}+\frac{\partial u_j(x,y,z,t)}{\partial x_i}-\frac{\delta_{ij}}{3}\frac{\partial u_k(x,y,z,t)}{\partial x_k}\right]+K(z)\delta_{ij}\times$$

$$\times\frac{\partial u_k(x,y,z,t)}{\partial x_k}-\beta(z)K(z)[T(x,y,z,t)-T_r],$$

$\rho(z)$ is the density of materials of heterostructure, δ_{ij} Is the Kronecker symbol. Conditions for the system of Eqs. (8) could be written in the form

$$\frac{\partial\vec{u}(0,y,z,t)}{\partial x}=0;\ \frac{\partial\vec{u}(L_x,y,z,t)}{\partial x}=0;\ \frac{\partial\vec{u}(x,0,z,t)}{\partial y}=0;\ \frac{\partial\vec{u}(x,L_y,z,t)}{\partial y}=0;$$

$$\frac{\partial\vec{u}(x,y,0,t)}{\partial z}=0;\ \frac{\partial\vec{u}(x,y,L_z,t)}{\partial z}=0;\ \vec{u}(x,y,z,0)=\vec{u}_0;$$

$$\vec{u}(x,y,z,\infty)=\vec{u}_0.$$

We calculate spatio-temporal distributions of concentrations of dopant and radiati-on defects by solving the Eqs. (1), (3), (5) and (8) framework standard method of averaging of function corrections [28]. Framework this paper we determine concentration of dopant, concentrations of radiation defects and components of displacement vector by using the second-order approximation framework method of averaging of function corrections. This approximation is usually enough good approximation to make qualitative analysis and to obtain some quantitative results. All obtained results have been checked by comparison with results of numerical simulations.

Discussion

In this section we analyzed dynamics of redistributions of dopant and radiation defects during annealing and under influence of mismatch-induced stress and modification of porosity. Typical distributions of concentrations of dopant in heterostructures are presented on Figs. 2 and 3 for diffusion and ion types of doping, respectively. These distributions have been calculated for the case, when value of dopant diffusion coefficient in doped area is larger, than in nearest areas. The figures show, that inhomogeneity of heterostructure gives us possibility to increase compactness of concentrations of dopants and at the same time to increase homogeneity of dopant distribution in doped part of epitaxial layer. However framework this approach of manufacturing of bipolar transistor it is necessary to optimize annealing of dopant and/or radiation defects. Reason of this optimization is following. If annealing time is small, the dopant did not achieve any interfaces between materials of heterostructure. In this situation one cannot find any modifications of distribution of concentration of dopant. If annealing time is large, distribution of concentration of dopant is too homogenous. We optimize annealing time framework recently introduces approach [29-37]. Framework this criterion we approximate real distribution of concentration of dopant by step-wise function (see Figs. 4 and 5). Farther we determine optimal values of annealing time by minimization of the following mean-squared error

$$U=\frac{1}{L_xL_yL_z}\int_0^{L_x}\int_0^{L_y}\int_0^{L_z}[C(x,y,z,\Theta)-\psi(x,y,z)]dzdydx \quad (15)$$

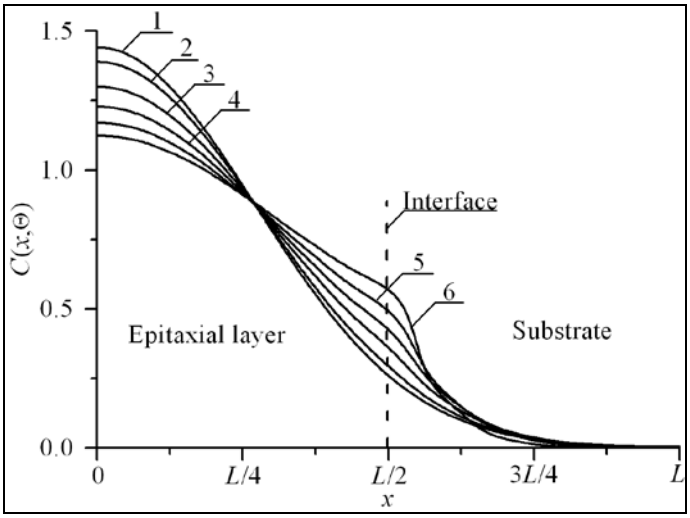

Fig 2: Distributions of concentration of infused dopant in heterostructure from Fig. 1 in direction, which is perpendicular to interface between epitaxial layer substrate. Increasing of number of curve corresponds to increasing of difference between values of dopant diffusion coefficient in layers of heterostructure under condition, when value of dopant diffusion coefficient in epitaxial layer is larger, than value of dopant diffusion coefficient in substrate

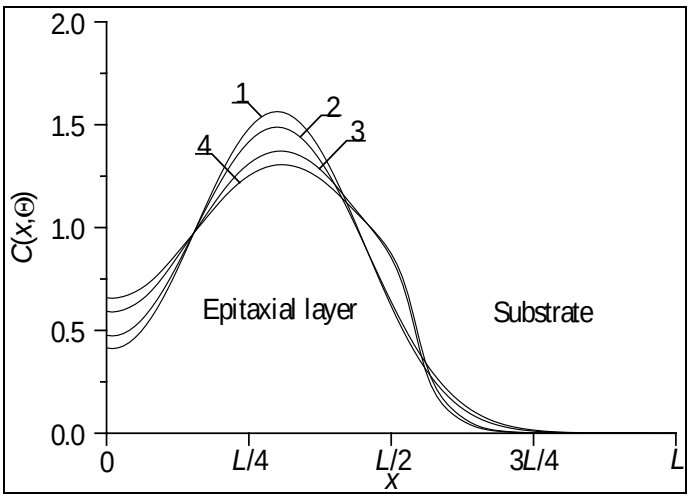

Fig 3: Distributions of concentration of implanted dopant in heterostructure from Fig. 1 in direction, which is perpendicular to interface between epitaxial layer substrate. Curves 1 and 3 corresponds to annealing time $\Theta = 0.0048(L_x^2+L_y^2+L_z^2)/D_0$. Curves 2 and 4 corresponds to annealing time $\Theta = 0.0057(L_x^2+L_y^2+L_z^2)/D_0$. Curves 1 and 2 corresponds to homogenous sample. Curves 3 and 4 corresponds to heterostructure under condition, when value of dopant diffusion coefficient in epitaxial layer is larger, than value of dopant diffusion coefficient in substrate

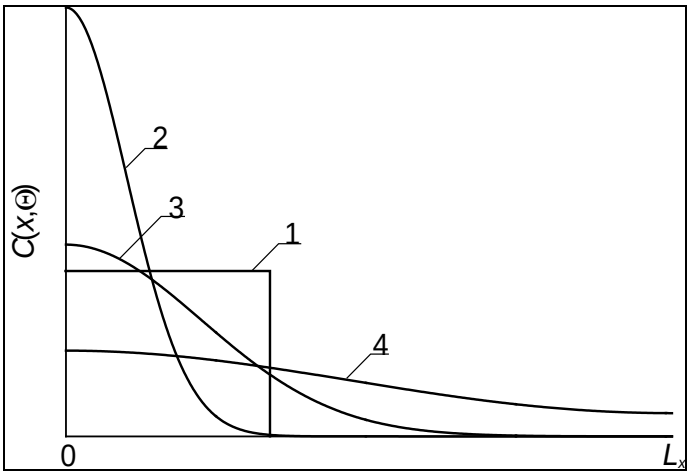

Fig 4: Spatial distributions of dopant in heterostructure after dopant infusion. Curve 1 is idealized distribution of dopant. Curves 2-4 are real distributions of dopant for different values of annealing time. Increasing of number of curve corresponds to increasing of annealing time

Where ψ (x, y, z) is the approximation function. Dependences of optimal values of annealing time on parameters are presented on Figs. 6 and 7 for diffusion and ion types of doping, respectively. It should be noted, that it

is necessary to anneal radiation defects after ion implantation. One could find spreading of concentration of distribution of dopant during this annealing. In the ideal case distribution of dopant achieves appropriate interfaces between materials of heterostructure during annealing of radiation defects. If dopant did not achieves any interfaces during annealing of radiation defects, it is practicably to additionally anneal the dopant. In this situation optimal value of additional annealing time of implanted dopant is smaller, than annealing time of infused dopant.

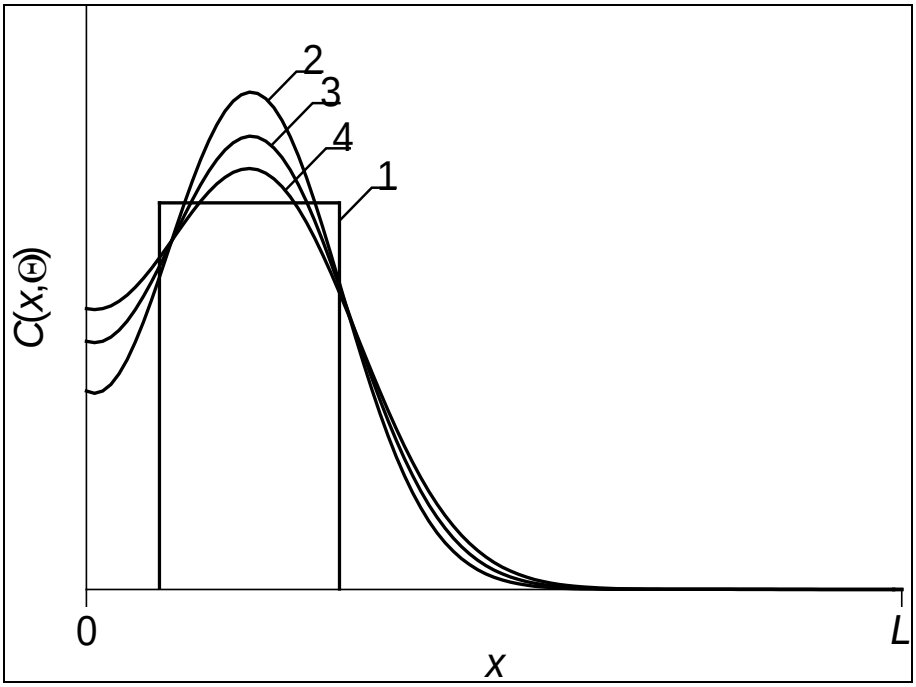

Fig 5: Spatial distributions of dopant in heterostructure after ion implantation. Curve 1 is idealized distribution of dopant. Curves 2-4 are real distributions of dopant for different values of annealing time. Increasing of number of curve corresponds to increasing of annealing time

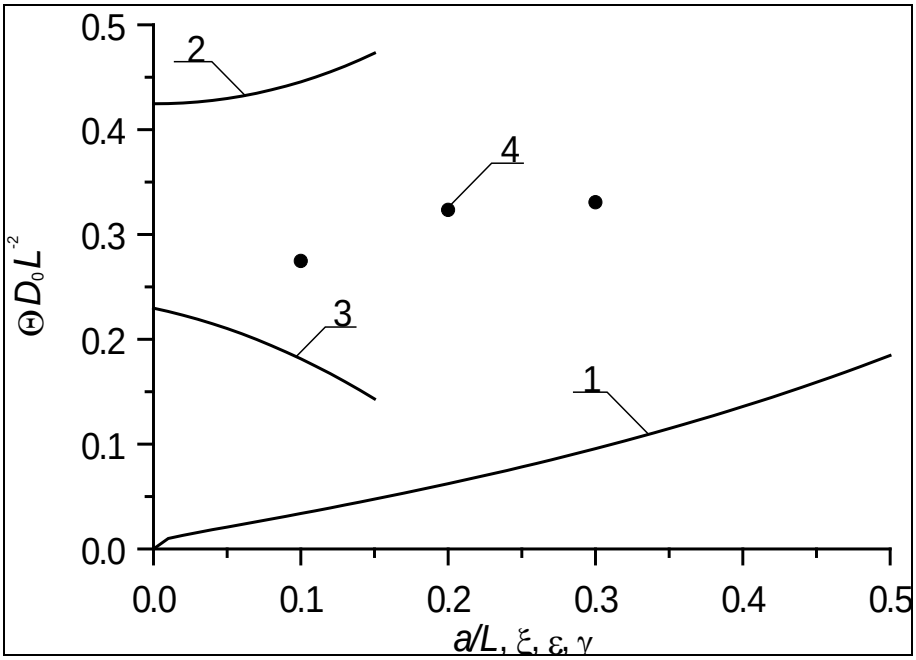

Fig 6: Dependences of dimensionless optimal annealing time for doping by diffusion, which have been obtained by minimization of mean-squared error, on several parameters. Curve 1 is the dependence of dimensionless optimal annealing time on the relation a/L and $\xi = \gamma = 0$ for equal to each other values of dopant diffusion coefficient in all parts of heterostructure. Curve 2 is the dependence of dimensionless optimal annealing time on value of parameter ε for a/L=1/2 and $\xi = \gamma = 0$. Curve 3 is the dependence of dimensionless optimal annealing time on value of parameter ξ for a/L=1/2 and $\varepsilon = \gamma = 0$. Curve 4 is the dependence of dimensionless optimal annealing time on value of parameter γ for a/L=1/2 and $\varepsilon = \xi = 0$

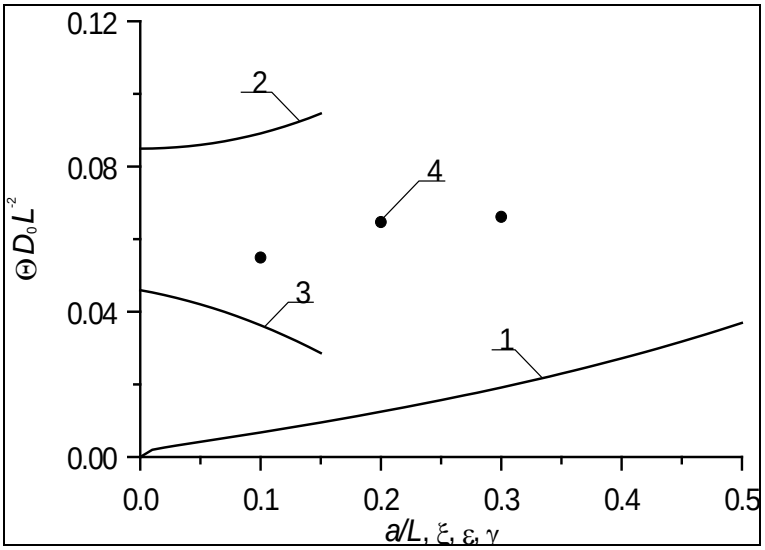

Fig 7: Dependences of dimensionless optimal annealing time for doping by ion implantation, which have been obtained by minimization of mean-squared error, on several parameters. Curve 1 is the dependence of dimensionless optimal annealing time on the relation a/L and $\xi = \gamma = 0$ for equal to each other values of dopant diffusion coefficient in all parts of heterostructure. Curve 2 is the dependence of dimensionless optimal annealing time on value of parameter ε for a/L=1/2 and $\xi = \gamma = 0$. Curve 3 is the dependence of dimensionless optimal annealing time on value of parameter ξ for a/L=1/2 and $\varepsilon = \gamma = 0$. Curve 4 is the dependence of dimensionless optimal annealing time on value of parameter γ for a/L=1/2 and $\varepsilon = \xi = 0$

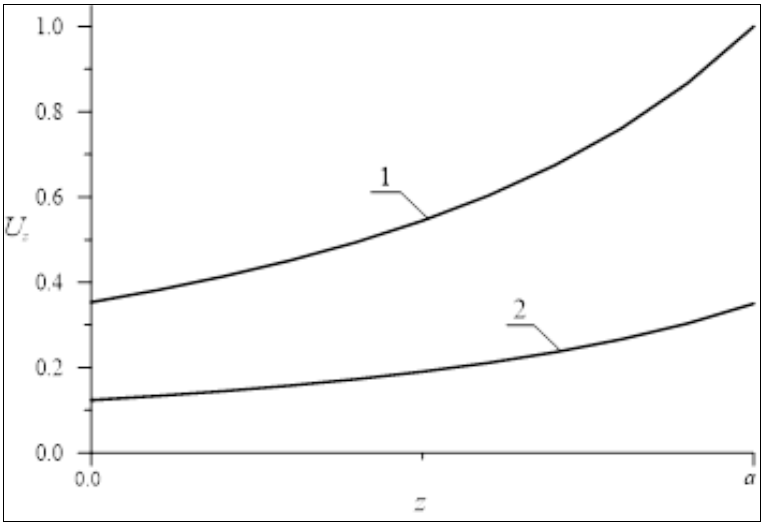

Fig 8: Normalized dependences of component u_z of displacement vector on coordinate z for nonporous (curve 1) and porous (curve 2) epitaxial layers

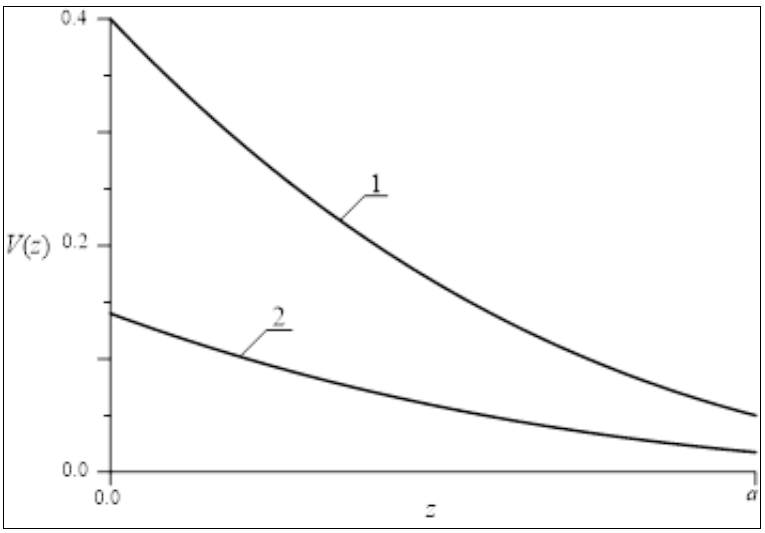

Fig 9: Normalized dependences of vacancy concentrations on coordinate z in unstressed (curve 1) and stressed (curve 2) epitaxial layers

Farther we analyzed influence of relaxation of mechanical stress on distribution of dopant in doped areas of heterostructure. Under following condition $\varepsilon_0 < 0$ one can find compression of distribution of concentration of dopant near interface between materials of heterostructure. Contrary (at $\varepsilon_0 > 0$) one can find spreading of distribution of concentration of dopant in this area. This changing of distribution of concentration of dopant could be at least partially compensated by using laser annealing [37]. This type of annealing gives us possibility to accelerate diffusion of dopant and another processes in annealed area due to in homogenous distribution of temperature and Arrhenius law. Accounting relaxation of mismatch-induced stress in heterostructure could leads to changing of optimal values of annealing time. At the same time modification of porosity gives us possibility to decrease value of mechanical stress. On the one hand mismatch-induced stress could be used to increase density of elements of integrated circuits. On the other hand could leads to generation dislocations of the discrepancy. Figs. 8 and 9 show distributions of concentration of vacancies in porous materials and component of displacement vector, which is perpendicular to interface between layers of heterostructure.

Conclusion

In this paper we model redistribution of infused and implanted dopants with account relaxation mismatch-induced stress during manufacturing field-effect heterotransistors framework a four stages distributed amplifier. We formulate recommendations for optimization of annealing to decrease dimensions of transistors and to increase their density. We formulate recommendations to decrease mismatch-induced stress. Analytical approach to model diffusion and ion types of doping with account concurrent changing of parameters in space and time has been introduced. At the same time the approach gives us possibility to take into account nonlinearity of considered processes.

References

1. Lachin VI, Savelov NS. *Electronics*. Rostov-on-Don: Phoenix, 2001.
2. Polishscuk A. Modern Electronics. 2004;12:8-11.
3. Volovich G. Modern Electronics. 2006;2:10-17.
4. Kerentsev A, Lanin V. Power Electronics. 2008;1:34.
5. Ageev AO, Belyaev AE, Boltovets NS, Ivanov VN, Konakova RV, Kudrik Ya Ya, *et al*. Sachenko. Semiconductors. 2009;43(7):897-903.
6. Jung-Hui Tsai, Shao-Yen Chiu, Wen-Shiung Lour, Der-Feng Guo. Semiconductors. 2009;43(7):971-974.
7. Alexandrov OV, Zakhar'in AO, Sobolev NA, Shek EI, Makoviychuk MM, Parshin EO. Semiconductors. 1998;32(9):1029-1032.
8. Ermolovich IB, Milenin VV, Red'ko RA, Red'ko SM. Semiconductors. 2009;43(8):1016-1020.
9. Sinsermsuksakul P, Hartman K, Kim SB, Heo J, Sun L, Park HH, *et al*. Appl. Phys. Lett. 2013;102(5):053901-053905.
10. Reynolds JG, Reynolds C Jr, Mohanta A, Muth JF, Rowe JE, Everitt HO, *et al*. Appl. Phys. Lett. 2013;102(15):152114-152118.
11. Volokobinskaya NI, Komarov IN, Matyukhina TV, Reshetnikov VI, Rush AA, Falina IV, *et al*. Semiconductors. 2001;35(8):1013-1017.
12. Pankratov EL, Bulaeva EA. Reviews in Theoretical Science. 2013;1(1):58-82.
13. Kukushkin SA, Osipov AV, Romanychev AI. Physics of the Solid State. 2016;58(7):1448-1452.
14. Trukhanov EM, Kolesnikov AV, Loshkarev ID. Russian Microelectronics. 2015;44(8):552-558.
15. Pankratov EL, Bulaeva EA. Reviews in Theoretical Science. 2015;3(4):365-398.
16. Ong KK, Pey KL, Lee PS, Wee ATS, Wang XC, Chong YF. Appl. Phys. Lett. 2006;89(17):172111-172114.
17. Wang HT, Tan LS, Chor EF. J. Appl. Phys. 2006;98(9):094901-094905.
18. Yu V, Bykov AG, Yeremeev NA, Zharova IV, Plotnikov KI, Rybakov MN, *et al*. Skupov. Radiophysics and Quantum Electronics. 2003;43(3):836-843.
19. Piccinni G, Avitabile G, Talarico C, Coviello G. Analog. Integr. Circ. Sig. Process. 2017;90:615-624.
20. Zhang YW, Bower AF. Journal of the Mechanics and Physics of Solids. 1999;47(11):2273-2297.
21. Landau LD, Lefshits EM. *Theoretical physics*. 7 (*Theory of elasticity*) Physmatlit, Moscow, 2001.
22. Kitayama M, Narushima T, Carter WC, Cannon RM, Glaeser AM. J. Am. Ceram. Soc. 2000;83:2561.
23. Kitayama M, Narushima T, Glaeser AM. J. Am. Ceram. Soc. 2000;83:2572.
24. Cheremskoy PG, Slesov VV, Betekhtin VI. Pore in solid bodies (Energoatomizdat, Moscow, 1990.
25. Yu Gotra Z. Technology of microelectronic devices Radio and communication, Moscow, 1991.
26. Fahey PM, Griffin PB, Plummer JD. Rev. Mod. Phys. 1989;61(2):289-388.
27. Vinetskiy VL, Kholodar' GA. Radiative physics of semiconductors. "Naukova Dumka", Kiev, 1979.
28. Mynbaeva MG, Mokhov EN, Lavrent'ev AA, Mynbaev KD, Techn. Phys. Lett. 2008;34(17):13.
29. Yu D. Sokolov. Applied Mechanics. 1955;1(1):23-35.
30. Pankratov EL. Russian Microelectronics. 2007;36(1):33-39.
31. Pankratov EL. Int. J. Nanoscience. 2008;7(4-5):187-197.
32. Pankratov EL, Bulaeva EA. Reviews in Theoretical Science. 2013;1(1):58-82.
33. Pankratov EL, Bulaeva EA. Int. J. Micro-Nano Scale Transp. 2012;3(3):119-130.
34. Pankratov EL, Bulaeva EA. International Journal of Modern Physics B. 2015;29(5):1550023-1-1550023-12.
35. Pankratov EL. J. Comp. Theor. Nanoscience. 2017;14(10):4885-4899.
36. Pankratov EL, Bulaeva EA. Materials science in semiconductor processing. 2015;34:260-268.
37. Pankratov EL, Bulaeva EA. Int. J. Micro-Nano Scale Transp. 2014;4(1):17-31.
38. Pankratov EL. Nano. 2011;6(1):31-40.